Bioconversion of Carbon Monoxide to Formate Using Artificially Designed Carbon Monoxide:Formate Oxidoreductase in Hyperthermophilic Archaea

Jae Kyu Lim (j.k.lim@kiost.ac.kr)
Korea Institute of Ocean Science & Technology (KIOST)
Ji-In Yang
Korea Institute of Ocean Science & Technology (KIOST)
Yun Jae Kim
Korea Institute of Ocean Science & Technology (KIOST)
Yeong-Jun Park
Korea Institute of Ocean Science & Technology (KIOST)
Yong Hwan Kim
Ulsan National Institute of Science and Technology (UNIST)

Article

Keywords: Bioconversion, carbon monoxide, oxidoreductase, hyperthermophilic archaea, metabolic engineering, electron, circuits, redox efficiency

Posted Date: October 13th, 2021

DOI: https://doi.org/10.21203/rs.3.rs-132617/v1

Version of Record: A version of this preprint was published at Communications Biology on June 3rd, 2022. See the published version at https://doi.org/10.1038/s42003-022-03513-7.

Bioconversion of carbon monoxide to formate using artificially designed carbon monoxide:formate oxidoreductase in hyperthermophilic archaea

Jae Kyu Lim[1]*, Ji-In Yang[1,2], Yun Jae Kim[1], Yeong-Jun Park[1,2], and Yong Hwan Kim[3]

[1]Korea Institute of Ocean Science and Technology, Busan 49111, Republic of Korea
[2]KIOST School, University of Science and Technology, Daejeon 34113, Republic of Korea
[3]School of Energy and Chemical Engineering, Ulsan National Institute of Science and Technology (UNIST), Ulsan 44919, Republic of Korea

Running title: Direct electron transfer by a FeS-FeS fusion protein

*For correspondence E-mail: j.k.lim@kiost.ac.kr

Abstract

Ferredoxin-dependent metabolic engineering of electron transfer circuits has been developed to enhance redox efficiency in the field of synthetic biology, e.g., for hydrogen production and for reduction of flavoproteins or $NAD(P)^+$. Here, we present the bioconversion of carbon monoxide (CO) gas to formate via a synthetic CO:formate oxidoreductase (CFOR), designed as an enzyme complex for direct electron transfer between noninteracting CO dehydrogenase and formate dehydrogenase using an electron-transferring Fe-S fusion protein. The CFOR-introduced *Thermococcus onnurineus* mutant strains showed CO-dependent formate production *in vivo* and *in vitro*. The formate production rate from purified CFOR complex and specific formate productivity from the bioreactor were 348 ± 34 μmol/mg/min and 90.2 ± 20.4 mmol/g-cells/h, respectively. The CO-dependent CO_2 reduction/formate production activity of synthetic CFOR was confirmed, indicating that direct electron transfer between two unrelated dehydrogenases was feasible via mediation of the FeS-FeS fusion protein.

Electron transfer is central to various essential metabolic pathways. For example, the electron transport chain and Fe-S proteins are essential constituents of the respiratory complex in all life forms on Earth. Fe-S proteins, which are involved in enzyme catalysis, regulation, maintenance of protein structure, and biological electron transfer[1,2], include [2Fe-2S], [3Fe-4S], and [4Fe-4S] types[1,3–5]. Quantum-mechanical electron transfer between two Fe-S clusters could explain the maximum distance of 14 Å for physiologically relevant electron tunneling[6]. Ferredoxins are small (~11 kDa) soluble electron carriers that bind to proteins that contain electrons held by reduced Fe-S clusters, providing unique opportunities for engineering and synthetic biology applications[7–13]. Artificial fusion of Fe-S proteins, such as ferredoxin and thioredoxin-like proteins, has been performed to improve electron transfer between redox partners[7–10,14–16]. Despite the reliable efficiency of protein fusion for facilitating electron transfer, target enzymes of fusion constructs are restricted to specific redox pairs that naturally interact with each other, such as ferredoxin and ferredoxin-dependent hydrogenase. Thus, a novel synthetic electron transferring path between two noninteracting redox enzymes has not yet been reported.

Hyperfine magnetic field generation at a reduced Fe-S cluster was first observed by Johnson *et al.,*[17] and it was applied to the synthesis of a novel electron transfer path in this study as a significant concept described in the 'Discussion' section. Subsequently, we attempted direct electron transfer between two different oxidoreductases, carbon monoxide dehydrogenase (CODH) and formate dehydrogenase (FDH), as a model system. CODH and FDH catalyze oxidoreduction of CO/CO_2 and formate/CO_2, respectively[18–24]. Theoretically, the overall reaction of the oxidation of CO to CO_2 with the reduction of CO_2 to formate is thermodynamically exergonic ($\Delta G'^{o}$ = -16.5 kJ/mol). CO oxidation coupled with CO_2 reduction to formate by connecting CODH and FDH is an ideal system for monitoring electron flow between the two redox enzymes. The electric current can be easily read-out as formate, and the overall reaction does not require an additional substrate other than only CO. We chose the carboxydotrophic and formatotrophic euryarchaeota *Thermococcus onnurineus* NA1, which harbors genes encoding both CODH and FDH (*codhB* and *fdhA*, respectively) and shows high cell resistance against both CO and formate[25–27], as a model organism. Notably, the hydrogen-dependent CO_2 reductase (HDCR) enzyme complex catalyzes CO_2 reduction to formate in *Acetobacterium woodii* using

hydrogen directly or coupled CODH-ferredoxin indirectly as an electron donor[28]. However, no natural enzymes have been shown to catalyze direct CO oxidation coupled with formate production.

Here, we constructed synthetic carbon monoxide:formate oxidoreductase (CFOR) for direct electron transfer between CODH and FDH using an electron-transferring Fe-S fusion protein in *T. onnurineus*. The synthetic CFOR complex was purified and assayed to assess electron transfer ability *in vivo* and *in vitro*.

Results

Construction of CO/formate bioconversion mutants via molecular fusion of two Fe-S proteins

The redox proteins CODH and FDH from *T. onnrineus* NA1 were engineered systematically through molecular fusion of electron-transferring Fe-S proteins to construct a single redox complex. The *codh* and *fdh3* gene clusters included the *codhABCD* and *focA-fdh3ABC* genes, respectively[25,29] (Fig. 1a and Supplementary Table 3). CodhA and Fdh3B are homologous to the FDH-N β subunit, FdnH (PDB 1FDI), in *E. coli*. FdnH has electron-transferring 4[4Fe-4S] clusters, and its amino acid sequence repeats the common motif for [4Fe-4S] cluster binding (CxxCxxCxnCP) or its slight variants[22]. Sequence alignment of FdnH showed that the [4Fe-4S] cluster binding motifs were identical to Fdh3B and CodhA (Supplementary Fig. 1a). However, Fdh3C showed high similarity with the 2[4Fe-4S] cluster binding motif in ferredoxins (Supplementary Fig. 1b). The results suggested that Fdh3B and CodhA or Fdh3C had an extrinsic domain with 4[4Fe-4S] or 2[4Fe-4S] clusters, respectively. Protein structure and *in silico* analyses suggest that FDH small subunits (Fdh3B homolog) directly interact with the FDH catalytic subunit (Fdh3A homolog) and another Fe-S protein (Fdh3C homolog)[22,30,31]. Therefore, Fdh3B was predicted to transfer electrons from Fdh3A to Fdh3C by connecting them in the complex. The amino acid sequences of CodhAB were also homologous to the CooFS proteins (41.7% and 50.3% identity, respectively) in *Rhodospirillum rubrum*. CooF mediates electron transfer from the CODH catalytic subunit CooS to hydrogenase and interacts directly with CooS[32,33]; hence, spontaneous enzyme complex formation of CodhA and CodhB is easily predictable. Accordingly, Fdh3C-CodhA and Fdh3B-CodhA were designed and constructed.

Fusion of Fe-S proteins led to the formation of novel protein complexes associated with CODH and FDH, termed synthetic CFOR. Therefore, the *fdh3B* or *fdh3C* genes were fused directly to the *codhA* gene using Gibson Assembly in two possible arrangements, *fdh3BC*:*codhA* and *fdh3B*:*codhA* (Fig. 1b and 1c). Structurally, the N- and C-termini of FdnH are located on the distal-end [4Fe-4S] cluster[22]; thus, the distal-end [4Fe-4S] cluster at each Fe-S protein was expected to be aligned face-to-face in every possible fusion combinations. Predicted models of the synthetic CFORs are presented in Supplementary Fig. 2. Next, the two flexible linkers $(GGGGS)_1$ and $(GGGGS)_2$ were designed with the

fdh3BC:*codhA* fusion arrangement. However, $(GGGGS)_3$ insertion was obtained during the homologous recombination of the $(GGGGS)_2$, resulting in three different lengths of linkers, which was confirmed by sequencing analysis. The *fdh3BC*:*codhA* fusion constructs pFd3CoL1C1118, pFd3CoL2C1119, and pFd3CoL3C1120 carried three different lengths of flexible linkers, i.e., $(GGGGS)_1$, $(GGGGS)_2$, and $(GGGGS)_3$, respectively (Supplementary Table 1). Notably, the shortest linker, $(GGGGS)_1$, showed the highest formate productivity (Supplementary Fig. 6b and 6c) and was selected for *fdh3B*:*codhA* fusion.

A fosmid vector was used to facilitate cloning for chromosomal insertion of the synthetic CFOR. Insertion of the expression construct was targeted to a region of the chromosome between convergent genes TON_1126 and TON_1127, as previously described[34]. A 9-kbp DNA fragment containing the *fdh3* and *codh* region and the P_{0157} promotor-HMG cassette was inserted into the chromosome of *T. onnurineus* D02 by transformation of pFd3CoL1C1118, pFd3CoL2C1119, and pFd3CoL3C1120, generating the mutant strains BCF01, BCF02, and BCF03, respectively (Fig. 1b). Strain BCF13 was then constructed by transformation of the pFd3NStrepCoL1C1149 fosmid, which contains the *fdh3B:codhA* fusion with $(GGGGS)_1$, into *T. onnurineus* D04 strain with additional deletion of the *fdh3* whole gene cluster (Fig. 1c and Supplementary Fig. 3a). An affinity-purification Strep-tag was also inserted within the operon at the N-terminus of *fdh3A* to allow easy purification of the synthetic CFOR enzyme at the strain BCF13 (Fig. 1c). Strain D05 was also constructed as a negative control for BCF13, which has no fusion linker between *fdh3B* and *codhA* (Supplementary Fig. 3b).

Determination of CO-dependent cell growth and formate production

Growth and metabolic profiles of the mutant strains were then compared. Initially, cell growth, formate production, and pH change were determined from *T. onnurineus* BCF01, which contained the fusion of *fdh3C:codhA* with the shortest length of $(GGGGS)_1$ linker. The growth rate of this strain was similar to that of the parental strain, whereas maximum cell growth was slightly reduced (Supplementary Fig. 4a). Cumulative formate production was detected during cell growth with a final concentration of 3.2 ± 0.2 mmol/L after 60 h of incubation for the BCF01 strain, whereas formate levels were below the detection

limit for the parental strain (Supplementary Fig. 4b). Based on the overall reaction, equivalent amounts of formate and H^+ are produced, thereby decreasing the pH during formate production. Indeed, the pH of the cell supernatant was significantly decreased from pH 6.9 to 5.0 only in the BCF01 strain (Supplementary Fig. 4c). This may affect sustainable formate production and cell growth, which are optimal at pH 6.5 under CO supplementation conditions[27]. Thus, 0.1 M bis-Tris propane (pH 6.5) buffer was added to the cell growth medium to prevent the abrupt pH change due to bioconversion of CO to formate, thus stabilizing the pH without growth inhibition (Supplementary Fig. 5).

Next, we compared the formate production ability of the remaining mutants. Cell growth was identical, and formate production was detected (Supplementary Fig. 6). BCF01 showed the highest formate production (7.5 mmol/L) after 60 h of incubation (Supplementary Fig. 6b). The relative formate productivities of BCF02 and BCF03 at the final time point were determined to be 78% and 84%, respectively, compared with BCF01 (Supplementary Fig. 6c). The $(GGGGS)_1$ linker showed the highest formate productivity; however, the effect on the electron transfer efficiency was insignificant. BCF13, carrying the *fdh3B:codhA* fusion with the $(GGGGS)_1$ linker, showed 6.6 ± 2.1 mmol/L formate production under CO-supplemented cell growth within 24 h (Fig. 2a), which was higher than that of BCF01 (4.3 ± 0.4 mmol/L formate) at the same time. Cell growth was similar to the other strains (Fig. 2a). Therefore, all subsequent experiments were conducted using the BCF13 strain. Formate production from the cell suspension was also investigated in serum vials using the strain D05 (without fusion linker) and BCF13 (with fusion linker) at an OD_{600} of about 0.5, incubated at 80℃ in the presence of CO gas with 2 bar (gauge pressure) CO/CO_2 (50:50 v/v) or CO/N_2 (50:50 v/v) mix gas. Activity and stability of the cell suspensions were confirmed by H_2 productivity that showed similar values among strains and gas conditions (Fig. 2c). In the BCF13, 3.0 ± 0.27 mmol/L formate was produced after 60 min incubation under the CO/CO_2 mix gas (Fig. 2b). In contrast, when the headspace was filled with CO/N_2, only 0.3 ± 0.04 mmol/L formate was produced due to the low CO_2 partial pressure (Supplementary Fig. 7). Although the CO oxidation reaction provides the equivalent CO_2 requirement for the formate production, the additionally supplemented CO_2 enhances the CO_2 reduction/formate production reaction. In the D05, formate production was detected under CO/CO_2 mix gas as a concentration of 0.1

± 0.007 mmol/L at 60 min, which is 30-fold lower than the BCF13. The results indicate that electron transfer between CODH and FDH modules is achievable just by overexpression of the enzymes but extremely enhanced by a flexible fusion of FeS-FeS in the synthetic CFOR complex.

Purification of the synthetic CFOR complex

We then purified the CFOR enzyme complex isolated from strain BCF13 grown in a fed-batch bioreactor with CO-supplemented MM1 medium to activate the expression of genes controlled by the strong promoter P_{0157}, which induces robust transcription and translation under CO-supplemented growth conditions[35]. The CFOR complex was purified using a strep-tag fused to the N-terminus of the FDH catalytic subunit, Fdh3A, and then analyzed by SDS-PAGE. Fdh3A, CodhB, and Fdh3B-CodhA fusion subunits, were present, with apparent molecular masses of 76, 67, and 42 kDa, indicating that the FdhB-CodhA fusion protein spontaneously bound to CodhB and FdhA to form the CFOR complex (Fig. 3a). Protein bands consistent with the calculated molecular weights from deduced amino acid sequences were observed for all three subunits. The calculated size of Fdh3B-CodhA was 43,722 Da. The CFOR complex was further purified using size-exclusion chromatography, and the CFOR complex from gel filtration was eluted as a single major peak with an apparent mass of around 488 kDa (Fig. 3b and 3c). The three major bands of purified protein were identified by LC-MS/MS analysis by bands cut from the SDS-PAGE gel (Fig. 3a and Supplementary Table 4). The 76-kDa and 67-kDa protein bands were identified as FdhA and CodhB, respectively. The 42-kDa protein band was thought to be the FdhB-CodhA fusion protein, which was identified as two different proteins, i.e., Fdh3B and CodhA. The additionally inserted formate transporter FocA[36] could enhance the secretion of intracellular formate synthesized by the CFOR complex. CodhC (29,274 Da) and CodhD (7,678 Da) are hypothetical proteins predicted to be involved in the maturation of the catalytic subunit CodhB[37,38]. However, FocA, CodhC, and CodhD subunits were not detected in both the SDS-PAGE gel and by LC-MS/MS analyses. Thus, the entire CFOR complex was composed of the CO dehydrogenase catalytic subunit (CodhB),

FDH catalytic subunit (Fdh3A), and Fe-S fusion proteins (Fdh3B-CodhA) connecting the two catalytic subunits.

Catalytic properties of the CFOR enzyme complex

The activities of CODH and FDH from purified CFOR complex were determined individually. The isolated CFOR catalyzed CO oxidation with a specific activity of 2,209 ± 159 μmol/mg/min and formate oxidation with a specific activity of 369 ± 181 μmol/mg/min at 80℃ (Supplementary Table 5). The specific activity of FDH was lower than that of CODH; therefore, the reaction of FDH was expected to be a limiting factor for the rate of formate production in the overall CFOR reaction. To confirm direct electron transfer by the Fe-S fusion protein, we investigated whether the purified CFOR could catalyze CO oxidation/formate production without any other additional electron carriers. The enzyme indeed catalyzed formate production from CO/CO_2 (50:50 v/v) mix gas with a specific activity of 348 ± 34 μmol/mg/min (Fig. 4 and Supplementary Table 5). However, formate was below the detection limit under conditions with 100% CO or without CFOR enzyme (Fig. 4). The maximum activity of the purified CFOR was determined at pH 7.5 in 50 mM sodium phosphate buffer (Supplementary Fig. 8). The results demonstrated that the simple, flexible fusion of two Fe-S proteins enabled electron transfer between them, leading to the formation of novel enzymes by assembly of noninteracting redox enzymes. Another formate production enzyme, HDCR in *A. woodii*, which reduces CO_2 to formate using hydrogen, has a specific activity of 10 μmol/mg/min[28]; therefore, synthetic CFOR showed a 35-fold higher formate production rate than native HDCR.

Bioconversion of CO to formate in a bioreactor

The formate production potential of the strain was tested in a bioreactor where 100% CO was continuously fed with a flowrate of 0.02–0.122 vvm (CO volume/working volume/min). Supplementary Table 6 summarizes the bioreactor parameters for the *T. onnurineus* BCF13 strain. Formate production was detected at a concentration of 56.4 ± 6.4 mmol/L after fermentation for 6 h (Fig. 5b). The formate production rate and specific formate productivity were calculated as 13.1 ± 0.9 mmol/L/h and 90.2 ±

20.4 mmol/g-cells/h, respectively. Recently CO-dependent formate production by coupling of CODH, ferredoxin, and HDCR was reported using *A. woodii* as a whole-cell biocatalyst; the formate production rate was 0.28 mmol/L/h[39]. *T. onnurineus* NA1 and its derivatives mutants used in this study are a basic hydrogenogenic carboxydotroph that can grow on CO as an energy source via the CO-dependent respiratory gene cluster *codh-mch-mnh3*[25,27,29]. Thus, the BCF13 strain showed carboxydotrophic properties, such as H_2 and CO_2 production (Fig. 2c and 5c), and could grow under 100% CO conditions with the maximum specific growth rate (μ_{max}) of 0.621 ± 0.051 h^{-1} (Fig. 5a). This spontaneous CO_2 production by the CO-dependent respiration enhances the formate production in the bioreactor. Therefore, *T. onnurineus* BCF13 could be used as an industrial microorganism for the production of H_2 and formate simultaneously from CO.

Discussion

Fe-S proteins involved in the electron transfer chain have been well characterized, both structurally and functionally. Fe-S proteins in many oxidoreductase complexes are typically associated with a large subunit that has catalytic redox activity and forms an enzyme complex, such as respiratory complex I, FDH-N and formate hydrogenlyase in *E. coli*[22,30,40]. However, direct electron transfer between CODH and FDH has not yet been found in nature. Thus, if one could construct an electron transfer system between these two oxidoreductases, it could serve as a universal electron transfer system. Accordingly, we generated fusion proteins between CodhA and Fdh3B to create a novel electron transfer path. The small subunits CodhA and Fdh3B specifically interacted with their catalytic large subunits. Therefore, the molecular fusion of Fe-S proteins may spontaneously mediate the formation of a novel CODH-FDH protein complex. However, a simple fusion between Fe-S proteins may not allow electron transfer. According to the electron tunneling theory, the maximum distance between the distal end [Fe-S] clusters at each protein must provide a distance of at least 14 Å for electron transfer, indicating that tight-binding and a sophisticated rearrangement of the two proteins are essential.

We showed that electron transfer was possible by simple fusion of the flexible (GGGGS) linker between electron-transferring Fe-S proteins. Based on the result, we suggest that the hyperfine magnetic field may affect this phenomenon. Indeed, Johnson *et al.* reported that the iron nuclei in the [Fe-S] cluster showed a magnetic hyperfine interaction with an electron spin S of $_{1/2}$, producing an effective field of about 180 kG in the reduced state[17]. Therefore, we hypothesized that the [4Fe-4S] clusters located at both distal ends of the Fe-S fusion protein would combine tightly by physical magnetic interaction, providing the electron tunneling condition. Accordingly, we propose the following model for the CO oxidation and formate production-coupled bioactivity of the artificially constructed CFOR complex by simple, flexible fusion of two Fe-S proteins (Fig. 6). First, there was no CO oxidation reaction in the initial; CodhA and FdhB were connected by a flexible linker but could not bind tightly, and hence, there was no electron transfer occurring based on the electron tunneling theory. Additionally, when the CO oxidation reaction began in CodhB, the distal-end [4Fe-S4] cluster at CodhA was reduced by electron transfer, leading to generation of a hyperfine magnetic field on the [4Fe-4S] cluster.

Moreover, another fused Fe-S protein, Fdh3B, was forced into the magnetic field by the flexible linker. Next, the ferromagnetic Fe atoms in the distal-end [4Fe-4S] cluster at Fdh3B were magnetized based on the influence of the magnetic field, thus binding tightly and rearranging with the [4Fe-4S] cluster of CodhA to provide the electron tunneling distance. Finally, electrons could be transferred from CODH to FDH through CodhA-Fdh3B fusion protein. Therefore, the synthetic CFOR complex catalyzes the CO_2 reduction/formate production reaction. However, no previous reports have described an attempt to transfer electrons directly between noninteracting proteins. Here, we developed a FeS-FeS fusion protein to provide a novel electron transfer path for the production of formate from CO by the synthetic CFOR enzyme complex in hyperthermophilic archaea. The electron transfer strategy endeavored here is based on an elementary natural phenomenon that 'Iron is attracted to a magnet.' This approach also exploited the self-assembly and self-regenerating abilities of live cells to create a novel formate production species. Overall, our results provide important insights into the synthesis of a new electron path using synthetic biology-based metabolic engineering. We focused on the possibility of electron transfer between noninteracting Fe-S proteins in this study. However, the effect of introducing various fusion combinations among Fe-S proteins and oxidoreductases remains to be determined for the broad application of this approach.

Acknowledgements

This work was supported by the KIOST In-house Program (PE99822) of the Ministry of Ocean and Fisheries, and the C1 Gas Refinery Program (2015M3D3A1A01064919) through the National Research Foundation of Korea (NRF) funded by the Ministry of Science, ICT & Future Planning. We thank Dr. Kae Kyoung Kwon, Dr. Jung-Hyun Lee, and Dr. Sung Gyun Kang at Marine Biotechnology Research Center, KIOST for supporting this research at the early stage as well as a critical discussion.

Author's contribution

J.K.L. conceptualized the study and study design. The experimental investigation was carried out by J.K.L., J.I.Y., Y.J.K., and Y.J.P. Data analysis was performed by J.K.L. and Y.J.K. Writing of the original draft and editing were carried out by J.K.L. Reviewing was carried out by Y.J.K. and Y.H.K. Supervision was done by J.K.L.

Competing interests

Patent applications describing the development and applications of CFOR and mutant strains to the KIOST and J.K.L., J.I.Y., Y.J.K., is accepted (no. 10-2129279 and 10-2129282) or pending (no. 10-2018-0138475 and PCT/KR 2018/014807).

References

1. Beinert, H., Holm, R. H. & Münck, E. Iron-sulfur clusters: nature's modular, multipurpose structures. *Science.* **277**, 653–659 (1997).
2. Cammack, R. & MacMillan, F. Electron magnetic resonance of iron–sulfur proteins in electron-transfer chains: resolving complexity. *Metals in Biology* 11–44 (Springer, New York, NY, 2010).
3. Rousset, M. *et al.* [3Fe-4S] to [4Fe-4S] cluster conversion in *Desulfovibrio fructosovorans* [NiFe] hydrogenase by site-directed mutagenesis. *Proc. Natl. Acad. Sci. U. S. A.* **95**, 11625–30 (1998).
4. Mouesca, J.-M. & Lamotte, B. Iron–sulfur clusters and their electronic and magnetic properties. *Coord. Chem. Rev.* **178**–**180**, 1573–1614 (1998).
5. Meyer, J. Iron–sulfur protein folds, iron–sulfur chemistry, and evolution. *JBIC J. Biol. Inorg. Chem.* **13**, 157–170 (2008).
6. Page, C. C., Moser, C. C., Chen, X. & Dutton, P. L. Natural engineering principles of electron tunnelling in biological oxidation–reduction. *Nature* **402**, 47–52 (1999).
7. Lacour, T. & Ohkawa, H. Engineering and biochemical characterization of the rat microsomal cytochrome P4501A1 fused to ferredoxin and ferredoxin–$NADP^+$ reductase from plant chloroplasts. *Biochim. Biophys. Acta - Protein Struct. Mol. Enzymol.* **1433**, 87–102 (1999).
8. Wittenberg, G., Sheffler, W., Darchi, D., Baker, D. & Noy, D. Accelerated electron transport from photosystem I to redox partners by covalently linked ferredoxin. *Phys. Chem. Chem. Phys.* **15**, 19608 (2013).
9. Agapakis, C. M. *et al.* Insulation of a synthetic hydrogen metabolism circuit in bacteria. *J. Biol. Eng.* **4**, 3 (2010).
10. Agapakis, C. M. & Silver, P. A. Modular electron transfer circuits for synthetic biology. *Bioeng. Bugs* **1**, 413–418 (2010).
11. Ducat, D. C., Way, J. C. & Silver, P. A. Engineering cyanobacteria to generate high-value products. *Trends Biotechnol.* **29**, 95–103 (2011).
12. Gilardi, G., Fantuzzi, A. & Sadeghi, S. J. Engineering and design in the bioelectrochemistry of metalloproteins. *Curr. Opin. Struct. Biol.* **11**, 491–499 (2001).

13. Agapakis, C. M., Boyle, P. M. & Silver, P. A. Natural strategies for the spatial optimization of metabolism in synthetic biology. *Nat. Chem. Biol.* **8**, 527–535 (2012).

14. Cao, P., Bülow, H., Dumas, B. & Bernhardt, R. Construction and characterization of a catalytic fusion protein system: P-45011β-adrenodoxin reductase-adrenodoxin. *Biochim. Biophys. Acta - Protein Struct. Mol. Enzymol.* **1476**, 253–264 (2000).

15. Sibbesen, O., De Voss, J. J. & Montellano, P. R. Putidaredoxin reductase-putidaredoxin-cytochrome $p450_{cam}$ triple fusion protein. Construction of a self-sufficient *Escherichia coli* catalytic system. *J. Biol. Chem.* **271**, 22462–9 (1996).

16. Bakkes, P. J. *et al.* Design and improvement of artificial redox modules by molecular fusion of flavodoxin and flavodoxin reductase from *Escherichia coli*. *Sci. Rep.* **5**, 12158 (2015).

17. Johnson, C. E., Bray, R. C., Cammack, R. & Hall, D. O. Mössbauer spectroscopy of the iron-sulfur proteins. *Proc. Natl. Acad. Sci. U. S. A.* **63**, 1234–1238 (1969).

18. Appel, A. M. *et al.* Frontiers, opportunities, and challenges in biochemical and chemical catalysis of CO2 fixation. *Chem. Rev.* vol. 113 6621–6658 (2013).

19. Ferry, J. G. CO dehydrogenase. *Annu. Rev. Microbiol.* **49**, 305–333 (1995).

20. Jeoung, J. H. & Dobbek, H. Carbon dioxide activation at the Ni,Fe-cluster of anaerobic carbon monoxide dehydrogenase. *Science.* **318**, 1461–1464 (2007).

21. Ferry, J. G. Formate dehydrogenase. *FEMS Microbiol. Rev.* **7**, 377–382 (1990).

22. Jormakka, M., Tornroth, S., Byrne, B. & Iwata, S. Molecular basis of proton motive force generation: structure of formate dehydrogenase-N. *Science.* **295**, 1863–1868 (2002).

23. Boyington, J. C., Gladyshev, V. N., Khangulov, S. V, Stadtman, T. C. & Sun, P. D. Crystal structure of formate dehydrogenase H: catalysis involving Mo, molybdopterin, selenocysteine, and an Fe_4S_4 cluster. *Science.* **275**, 1305–1308 (1997).

24. Popov, V. O. & Lamzin, V. S. NAD^+-dependent formate dehydrogenase. *Biochem. J.* **301**, 625–643 (1994).

25. Lee, H. S. *et al.* The complete genome sequence of *Thermococcus onnurineus* NA1 reveals a mixed heterotrophic and carboxydotrophic metabolism. *J. Bacteriol.* **190**, 7491–7499 (2008).

26. Lim, J. K. *et al.* Thermodynamics of formate-oxidizing metabolism and implications for H_2 production. *Appl. Environ. Microbiol.* **78**, 7393–7397 (2012).

27. Kim, M.-S. S. *et al.* CO-dependent H_2 production by genetically engineered *Thermococcus onnurineus* NA1. *Appl. Environ. Microbiol.* **79**, 2048–2053 (2013).

28. Schuchmann, K. & Müller, V. Direct and reversible hydrogenation of CO_2 to formate by a bacterial carbon dioxide reductase. *Science.* **342**, 1382–1385 (2013).

29. Lim, J. K., Kang, S. G., Lebedinsky, A. V, Lee, J.-H. & Lee, H. S. Identification of a novel class of membrane-bound [NiFe]-hydrogenases in *Thermococcus onnurineus* NA1 by *in silico* analysis. *Appl. Environ. Microbiol.* **76**, 6286–6289 (2010).

30. McDowall, J. S. *et al.* Bacterial formate hydrogenlyase complex. *Proc. Natl. Acad. Sci. U. S. A.* **111**, E3948–E3956 (2014).

31. Sauter, M., Bohm, R. & Bock, A. Mutational analysis of the operon (hyc) determining hydrogenase 3 formation in Escherichia coli. *Mol. Microbiol.* **6**, 1523–1532 (1992).

32. Bonam, D. & Ludden, P. W. Purification and characterization of carbon monoxide dehydrogenase, a nickel, zinc, iron-sulfur protein, from Rhodospirillum rubrum. *J. Biol. Chem.* **262**, 2980–2987 (1987).

33. Ensign, S. A. & Ludden, P. W. Characterization of the CO oxidation/H2 evolution system of Rhodospirillum rubrum. Role of a 22-kDa iron-sulfur protein in mediating electron transfer between carbon monoxide dehydrogenase and hydrogenase. *J. Biol. Chem.* **266**, 18395–18403 (1991).

34. Kim, M.-S. *et al.* A novel co-responsive transcriptional regulator and enhanced H_2 production by an engineered *Thermococcus onnurineus* NA1. *Appl. Environ. Microbiol.* **81**, 1708–1714 (2015).

35. Lee, S. H. *et al.* Comparison of CO-dependent H_2 production with strong promoters in *Thermococcus onnurineus* NA1. *Appl. Microbiol. Biotechnol.* **98**, 979–986 (2014).

36. Wang, Y. *et al.* Structure of the formate transporter FocA reveals a pentameric aquaporin-like channel. *Nature* **462**, 467–472 (2009).

37. Watt, R. K. & Ludden, P. W. Ni(2+) transport and accumulation in Rhodospirillum rubrum. *J. Bacteriol.* **181**, 4554–4560 (1999).

38. Jeon, W. B., Cheng, J. & Ludden, P. W. Purification and characterization of membrane-associated CooC protein and its functional role in the insertion of nickel into carbon monoxide dehydrogenase from Rhodospirillum rubrum. *J. Biol. Chem.* **276**, 38602–38609 (2001).

39. Hwang, H. W. *et al.* Two-stage bioconversion of carbon monoxide to biopolymers via formate as an intermediate. *Chem. Eng. J.* **389**, 124394 (2020).

40. Baradaran, R., Berrisford, J. M., Minhas, G. S. & Sazanov, L. A. Crystal structure of the entire respiratory complex I. *Nature* **494**, 443–8 (2013).

41. Bae, S. S. *et al.* *Thermococcus onnurineus* sp, nov., a hyperthermophilic archaeon isolated from a deep-sea hydrothermal vent area at the PACMANUS field. *J. Microbiol. Biotechnol.* **16**, 1826–1831 (2006).

42. Kim, Y. J. *et al.* Formate-driven growth coupled with H_2 production. *Nature* **467**, 352–355 (2010).

43. Sokolova, T. G. *et al.* The first evidence of anaerobic CO oxidation coupled with H_2 production by a hyperthermophilic archaeon isolated from a deep-sea hydrothermal vent. *Extremophiles* **8**, 317–323 (2004).

44. Sambrook, J., Fritsch, E. F. & Maniatis, T. Molecular cloning: a laboratory manual. *Mol. cloning a Lab. manual.* (1989).

45. Jeong, J.-Y. *et al.* One-step sequence-and ligation-independent cloning as a rapid and versatile cloning method for functional genomics studies. *Appl. Environ. Microbiol.* **78**, 5440–5443 (2012).

46. Jeon, J. H. *et al.* Characterization of the *frhAGB*-encoding hydrogenase from a non-methanogenic hyperthermophilic archaeon. *Extremophiles* **19**, 109–118 (2015).

47. Schmitz, R. P. & Diekert, G. Purification and properties of the formate dehydrogenase and characterization of the *fdhA* gene of *Sulfurospirillum multivorans*. *Arch Microbiol* **180**, 394–401 (2003).

48. Amend, J. P. & Shock, E. L. Energetics of overall metabolic reactions of thermophilic and hyperthermophilic Archaea and Bacteria. *FEMS Microbiol. Rev.* **25**, 175–243 (2001).

Figures

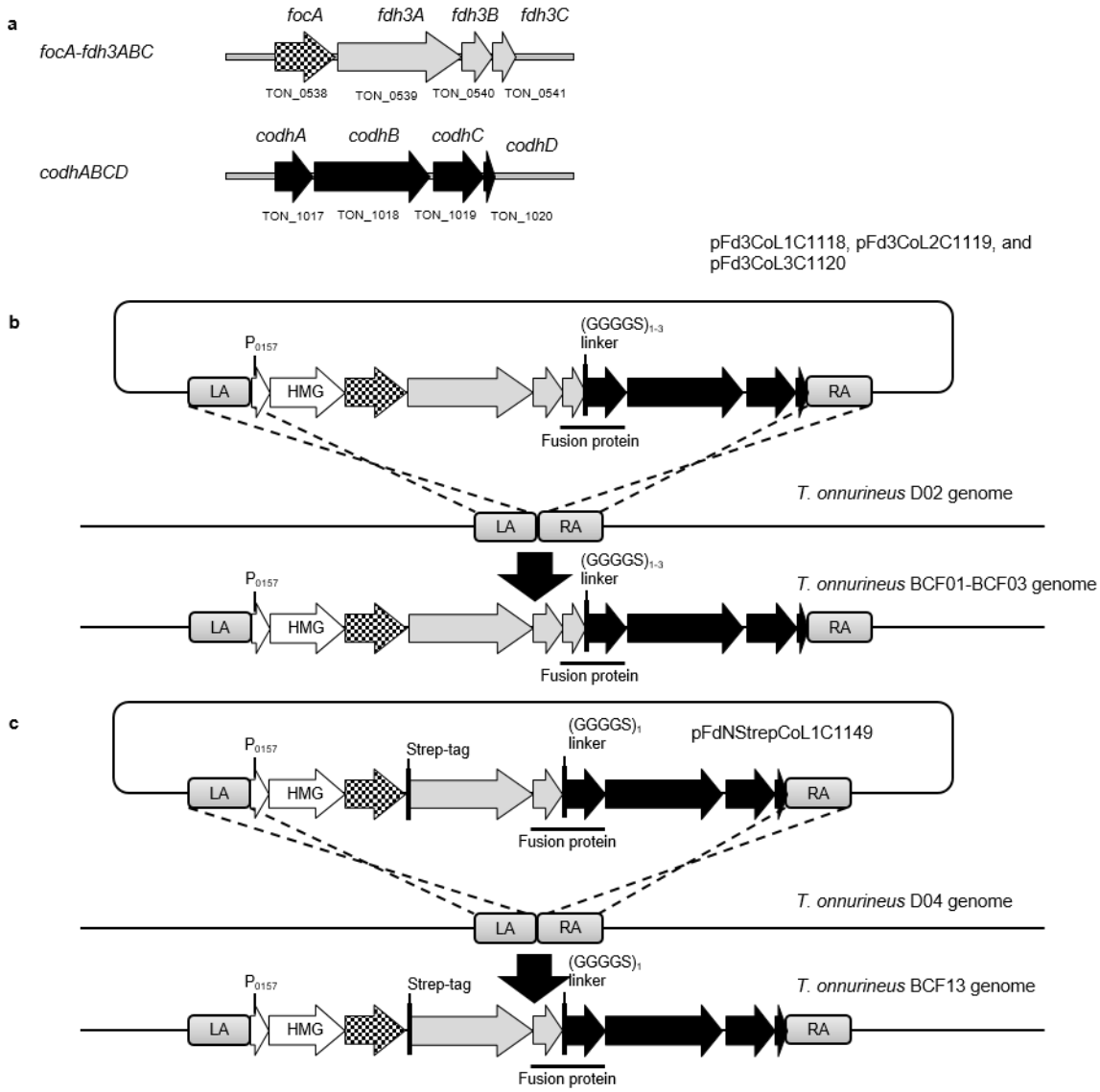

Figure 1. Construction of the CO-formate bioconversion mutants by cloning of the synthetic CFOR. a, Gene arrangement of the *fdh3* and *codh* gene clusters on the genome of *T. onnurineus* NA1. The name of genes and locus tags are indicated on the upper and lower side of the genes, respectively. **b**, Construction of *T. onnurineus* BCF01, BCF02, and BCF03 mutants by transformation and homologous recombination of the *fdh3C:codhA* fusion containing fosmids pFd3CoL1C1118 $(GGGGS)_1$, pFd3CoL1C1119 $(GGGGS)_2$, and pFd3CoL1C1120 $(GGGGS)_3$, respectively. **c**, Construction of *T. onnurineus* BCF13 mutant by the transformation of the fosmid

pFd3NStrepCoL1C1149, which contains a fusion of *fdh3B:codhA* with linker $(GGGGS)_1$ and strep-tag at the N-terminus of Fdh3A.

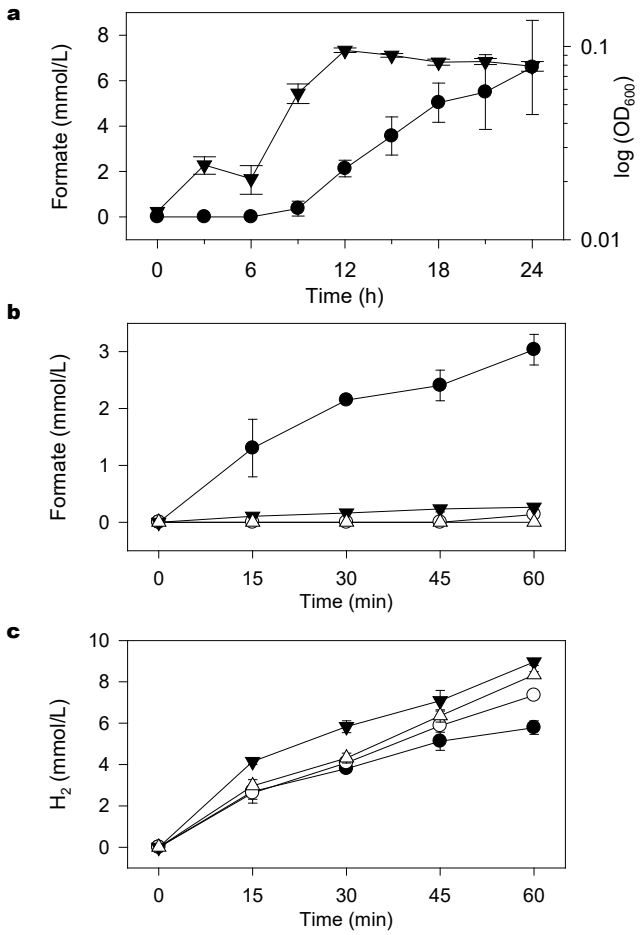

Figure 2. CO-dependent formate production. a, Formate production (●) and cell growth (▼) of *T. onnurineus* BCF13. Cells were cultured in MM1 medium supplemented with 0.1 M bis-Tris propane (pH 6.5) and 2 bar of CO gas at 80℃. **b and c**, Formate (**b**) and H_2 (**c**) production from cell suspensions of *T. onnurineus* BCF13 and *T. onnurineus* D05. Cells (OD_{600} = 0.5) were incubated with CO/CO_2 (50:50 v/v) mix gas or CO/N_2 (50:50 v/v) mix gas in modified PBS buffer at 80℃. Symbols: ●, BCF13 with CO/CO_2 mix gas; ○, D05 with CO/CO_2 mix gas; ▼, BCF13 with CO/N_2 mix gas; △, D05 with CO/N_2 mix gas. Error bars represent the standard deviations (n = 3).

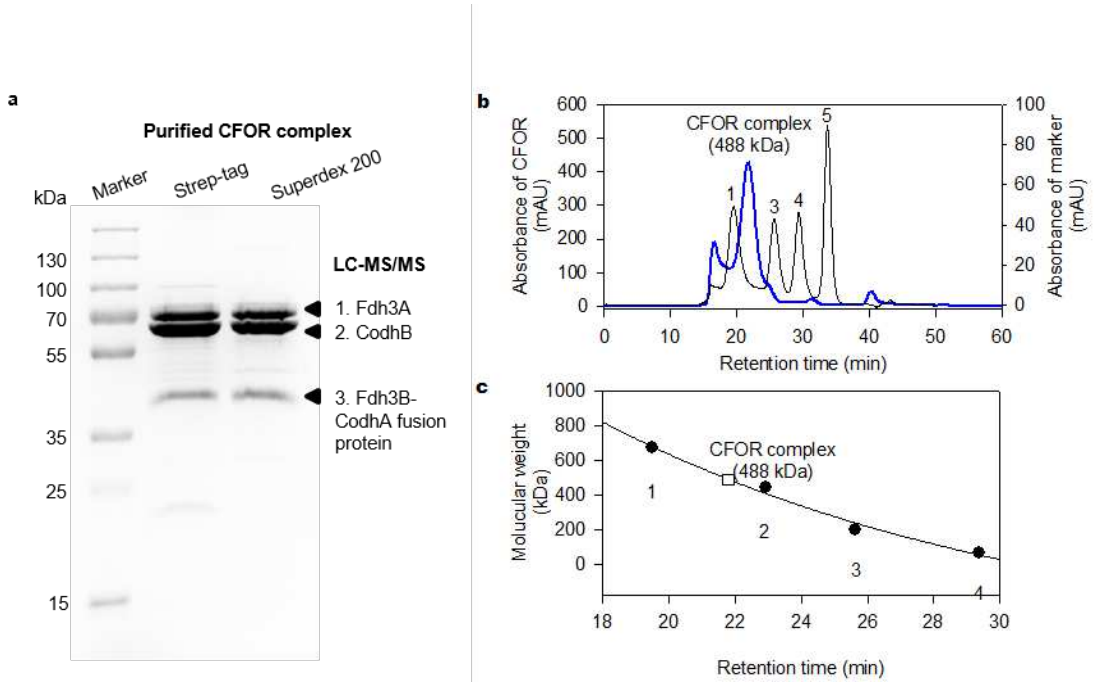

Figure 3. Purification and identification of the synthetic CFOR complex from *T. onnurineus* BCF13. a, Strep-tag purified CFOR complex (5 μg) was loaded to a 12% acrylamide gel and stained with Coomassie Brilliant Blue after gel running. CFOR subunits identified by LC-MS/MS are indicated with a black arrow. **b**, The affinity column purified CFOR complex (blue line), and standard marker (black line) were separated on a Superdex 200 10/300 GL column. A number on a standard peak indicates: 1. Thiroglobulin, 669 kDa; 2. Apoferritin, 443 kDa; 3. Beta-amylase, 200 kDa; 4. Albumin, 66 kDa; 5. Carbonic anhydrase, 29 kDa. **c**, The retention time versus the logarithm of the molecular weight of the CFOR complex (□) and standard marker (●) was plotted on the regression.

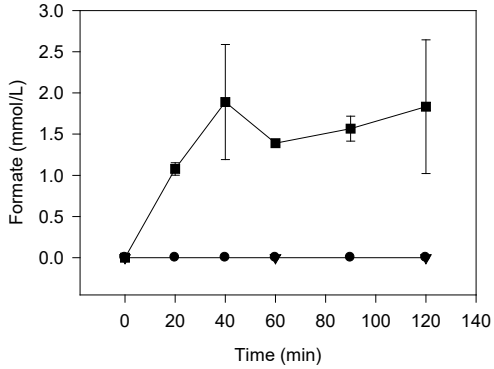

Figure 4. *In vitro* formate production by purified CFOR complex. The formate production was determined at the absence (●) or presence of 50 ug of purified CFOR complex that incubated with 2 bar (gauge pressure) of CO/CO_2 (50:50 v/v) (■) or 0.5 bar (gauge pressure) of 100% CO (▼) in 50 mM sodium phosphate buffer (pH 7.5). Formate production was determined by HPLC. Error bars represent the standard deviations (n = 3).

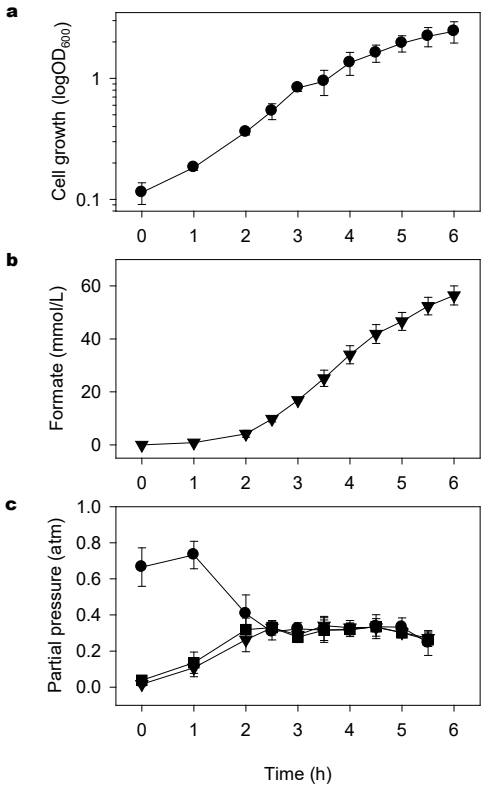

Figure 5. CO-dependent fed-batch culture in bioreactor. a, Cell growth was monitored by measuring OD_{600}. **b**, Formate production was determined by HPLC. **c**, Partial pressure of CO (●), CO_2 (▼) and H_2 (■) in headspace was determined by GC. CO (100%) was supplied with initial flow rate of 0.02 vvm and was raised to 0.122 vvm during the fed-batch culture. Error bars represent the standard deviations (n = 4).

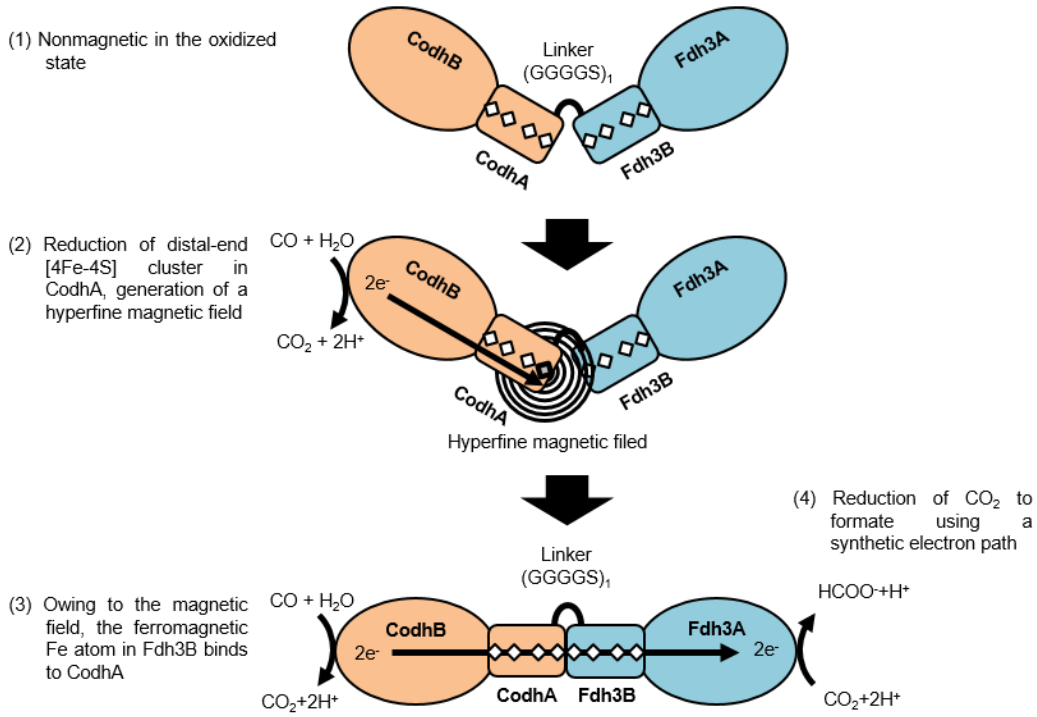

Figure 6. Proposed mechanism of electron transfer within Fe-S fusion protein by a hyperfine magnetic field.

Supplementary Table and Figure

Supplementary Table 1. Strains, plasmids and fosmids used this study.

Strains/Plasmids/Fosmids	Description	Reference
Strains		
E. coli		
EPI300^{TM}-T1^{R}	Fosmid cloning host	EPICENTRE
T. onnurineus		
NA1	Wild-type strain	[41]
D02	NA1 derivative, *Δfdh1* gene cluster (TON_0266-TON_0282) *Δfdh2* gene cluster (TON_1563-TON_1580) *Δfdh3A* (TON_0539)	Previous construction (not reported)
D04	D02 derivative, *Δfdh1* gene cluster (TON_0266-TON_0282) *Δfdh2* gene cluster (TON_1563-TON_1580) *Δfdh3* gene cluster (TON_0539-TON_0541)	This study
D05	D04 derivative pFd3StrepCodhC2008 transformation, P_{0157}*hmgpfu*::*focA-fdh3AB-codhABCD*; Strep-tag inserted in N-terminus of Fdh3A; control strain for the strain BCF13	This study
BCF01	D02 derivative pFd3CoL1C1118 transformation, P_{0157}*hmg*$_{pfu}$::*focA-fdh3ABC*:*codhABCD*; fusion of *fdh3C* and *codhA* with linker $(GGGGS)_1$	This study
BCF02	D02 derivative pFd3CoL2C1119 transformation, P_{0157}*hmg*$_{pfu}$::*focA-fdh3ABC*:*codhABCD*; fusion of *fdh3C* and *codhA* with linker $(GGGGS)_2$	This study

(Condinued)

Strains/Plasmids/Fosmids	Description	Reference
BCF03	D02 derivative pFd3CoL3C1120 transformation, P_{0157}*hmg*$_{pfu}$::*focA-fdh3ABC*:*codhABCD*; fusion of *fdh3C* and *codhA* with linker $(GGGGS)_3$	This study
BCF12	D04 derivative pFd3NHisCoL1C1132 transformation, P_{0157}*hmgpfu*::*focA-fdh3AB*:*codhABCD*; fusion of *fdh3B* and *codhA* with linker $(GGGGS)_1$; His-tag inserted in N-terminus of Fdh3A	This study
BCF13	D04 derivative pFd3NStrepHisCoL1C1149 transformation, P_{0157}*hmgpfu*::*focA-fdh3AB*:*codhABCD*; fusion of *fdh3B* and *codhA* with linker $(GGGGS)_1$; Strep-tag inserted in N-terminus of Fdh3A	This study
Plasmids		
pUC vector		
pUC118	Backbone plasmid; Amp^r	TAKARA
pFdh1,2,3clusterA1135	pUC118 carrying P_{gdh} promotor, HMG cassette, and 1kbp Left-arm (LA) and Right-arm (RA) for deletion of fdh3 gene cluster (TON_0539-TON_0541)	This study
Fosmids		
pCC1FOS	Backbone fosmid; Cm^r	EPICENTRE
pNA1comFosC1096	pCC1FOS carrying P_{0157} promotor, HMG cassette, and 1kbp Left-arm (LA) and Right-arm (RA) for homologous recombination of *T. onnurineus* NA1 genome; backbone fosmid for mutant construction; Sim^r	This study
pFd3CoL1C1118	pNA1comFosC1096 carrying *fdh3* region (*focA-fdh3ABC*) and *codh* region (*codhABCD*) from *T. onnurineus* NA1; fusion of *fdh3C* and *codhA* with linker $(GGGGS)_1$	This study

(Condinued)

Strains/Plasmids/Fosmids	Description	Reference
pFd3CoL2C1119	pFd3CoL1C1118 carrying fusion of *fdh3C* and *codhA* with linker $(GGGGS)_2$	This study
pFd3CoL3C1120	pFd3CoL1C1118 carrying fusion of *fdh3C* and *codhA* with linker $(GGGGS)_3$	This study
pFd3NHisCoL1C1132	pNA1comFosC1096 carrying *fdh3* region (*focA-fdh3AB*) and *codh* region (*codhABCD*) from *T. onnurineus* NA1; fusion of *fdh3B* and *codhA* with linker $(GGGGS)_1$; His_6-tag inserted in N-terminus of Fdh3A	This study
pFd3NHisStrepCoL1C1149	pNA1comFosC1096 carrying *fdh3* region (*focA-fdh3AB*) and *codh* region (*codhABCD*) from *T. onnurineus* NA1; fusion of *fdh3B* and *codhA* with linker $(GGGGS)_1$; pFd3NHisCoL1C1132 carrying Strep-tag inserted in N-terminus of Fdh3A (TON_0539)	This study
pFd3NStrepCodhC2008	pNA1comFosC1096 carrying *fdh3* region (*focA-fdh3AB*) and *codh* region (*codhABCD*) from *T. onnurineus* NA1 without fusion linker; Strep-tag inserted in N-terminus of Fdh3A (TON_0539)	This study

Supplementary Table 2. PCR primers used in this study. Bold and underlined nucleotides indicate (GGGGS)n linker and tagging sequences, respectively.

Construction/PCR	Nucleotide sequence (5' to 3')	
	Forward	**Reverse**
pNA1comFosC1096		
Left-arm-P_{0157}-*hmg*	AGCTCGGTACCCGGGGATCCCCAGACCCTCCTCGAGACGA	TGACGCCACGCATGCCTAGGTCATCTCCCAAGCATTTTATGAG
Right-arm	TGCTTGGGAGATGACCTAGGCATGCGTGGCGTCAACGATG	AGGTCGACTCTAGAGGATCCAATGGAATAACCCATCTCACGG
pFdh1,2,3clusterA1135		
Left-arm	AATTCGAGCTCGGTACCCGGGGATCCATGGCACAGAATAATTCACTCG	GGCCATCCTTAACAGCACCACCGCCCTATCTTC
Right-arm	GATAGGGCGGTGGTGCTGTTAAGGATGGCCTGTATG	CCAGTGCCAAGCTTGCATGCCTGCAGGAATGACCTTGGTTATGCCG
pFd3CoL1C1118		
focA-fdh3C:codhA$(GGGGS)_1$	TAAAATGCTTGGGAGATGACCTAGGATGGCACAGAATAATTCACTCG	GGCAT**GCTGCCTCCGCCGCC**CCCCCAGGTAAGCCTCATATTTG
fdh3C:codhA$(GGGGS)_1$-*codhD*	TGGGG**GGCGGCGGAGGCAGC**ATGCCAGCTTTTTCCGGTTC	TGGCCATCGTTGACGCCACGCATGCGACGTCTCACCTCCTGAGTTTAAACCTCAT
pFd3CoL2C1119		
focA-fdh3C:codhA$(GGGGS)_2$	TAAAATGCTTGGGAGATGACCTAGGATGGCACAGAATAATTCACTCG	**GCTGCCTCCGCCGCCGCTTCCGCCTCCTCC**CCCCAGGTAAGCCTCATATTTG
fdh3C:codhA$(GGGGS)_2$-*codhD*	**GGCGGCGGAGGCAGCGGAGGAGGCGGAAGC**ATGCCAGCTTTTCCGGTTC	TGGCCATCGTTGACGCCACGCATGCGACGTCTCACCTCCTGAGTTTAAACCTCAT
pFd3NHisCoL1C1132		
focA-His:fdh3A	TAAAATGCTTGGGAGATGACCTAGGATGGCACAGAATAATTCACTCG	TCCTCGTGATGGTGGTGATGGTGCATCCGCACCACCGCCCT
His:fdh3A-fdh3B:codhA$(GGGGS)_1$	GGATGCACCATCACCACCATCACGAGGAGTTTAAGATTGGCCTG	GCTGGGCTGCCTCCGCCGCCCCCGAAGTAGGCGAGCG
fdh3B:codhA$(GGGGS)_1$-*codhD*	TCGGGGGCGGCGGAGGCAGCCCAGCTTTTTCCGGTTCC	TGGCCATCGTTGACGCCACGCATGCGACGTCTCACCTCCTGAGTTTAAACCTCAT
pFd3NStrepCoL1C1149		
focA-Strep:fdh3A	TAAAATGCTTGGGAGATGACCTAGGATGGCACAGAATAATTCACTCG	TCCTCTGGTCCCACCCGCAGTTCGAGAAGCATCCGCACCACCGCCCT

Strep:fdh3A-codhD	GGATGCTTCTCGAACTGCGGGTGGGACCAGAGGAGTTTAAGATTGGCCTG	TGGCCATCGTTGACGCCACGCATGCGACGTCTCACCTCCTGAGTTTAAACCTCAT
pFd3NStrepCodhC2008		
focA-fdh3B	TAAAATGCTTGGGAGATGACCTAGGATGGCACAGAATAATTCACTCG	TGTTGATCACCTCGTTCACCCGAAGTAGGCGAGCG
codhA-codhD	GCCTACTTCGGGTGAACGAGGTGATCAACAATGCC	TGGCCATCGTTGACGCCACGCATGCGACGTCTCACCTCCTGAGTTTAAACCTCAT

Supplementary Table 3. Information of the proteins used in this study.

Proteins	Locug tag	M. W. (Da)	NCBI annotation
Fdh3			
FocA	TON_0538	35,570	Hypothetical formate transporter
Fdh3A	TON_0539	75,626	Hypothetical formate dehydrogenase, alpha subunit
Fdh3B	TON_0540	18,342	Oxidoreductase iron-sulfur protein
Fdh3C	TON_0541	13,925	4Fe-4S cluster-binding protein
Codh			
CodhA	TON_1017	23,581	4Fe-4S ferredoxin, iron-sulfur binding domain protein
CodhB	TON_1018	67,671	carbon-monoxide dehydrogenase, catalytic subunit
CodhC	TON_1019	29,274	Hypothetical ATP-binding protein
CodhD	TON_1020	7,678	Hypothetical RNA-binding protein

Supplementary Table 4. LC-MS/MS identification of purified CFOR subunits showing number of peptides matched and peptide sequence coverage.

Protein band	Subunit	Accession Number	NCBI Annotation	Predicted M.W. (Da)	Sequence coverage (%)	MASCOT Score
1	Fdh3A	gi|212008644	Hypothetical formate dehydrogenase, alpha subunit	76324	74	2602
2	CodhB	gi|212009124	Carbon-monoxide dehydrogenase, catalytic subunit	68715	79	2704
3	Fdh3B	gi|212008645	Oxidoreductase iron-sulfur protein	19243	81	844
3	CodhA	gi|212009123	4Fe-4S ferredoxin, iron-sulfur binding domain protein	24479	77	1141

Supplementary Table 5. Specific activities of CO oxidation, formate oxidation, and formate production by the purified CFOR.

Assay	Specific activities (μmol/mg/min)	Description
CO oxidation	2,209 ± 159	Methyl viologen as an electron acceptor
Formate oxidation	369 ± 181	Methyl viologen as an electron acceptor
Formate production	348 ± 34	CO dependent formate production

Supplementary Table 6. Bioreactor parameters of *T. onnurineus* BCF13.

Parameter	Value
Maximum specific growth rate, μ_{max} (h^{-1})[a]	0.621 ± 0.051
Formate production rate (mmol/L/h)[b]	13.1 ± 0.9
Specific formate productivity (mmol/g-cells/h)[b]	90.2 ± 20.4

[a] The μ_{max} was determined using the values of the linear regression slope in time windows of 1 to 4.5 hours.

[b] Values were determined by dividing total yield by time difference from 2 to 6 hours.

Supplementary Figure 1. Alignment of the amino acid sequence of Fe-S proteins within the CFOR in *T. onnurienus* (*To*) and other Fe-S proteins in which crystal structure has been determined. The conserved [4Fe-4S] cluster is boxed, and the position of conserved Cys residues are indicated as bold. **a**, Amino acid sequences of Fdh3B and CodhA subunits are aligned with 4[4Fe-4S] clusters

containing FdnH (PDB 1FDI) in *E. coli* (*Ec*). **b**, Multiple alignments of Fdh3C subunit was achieved with other 2[4Fe-4S] clusters containing ferredoxins (Fd) in *Clostridium acidurici* (*Ca*, PDB 1FDN), *Gottschalkia acidurici* (*Ga*, PDB 1FCA), *Clostridium pasteurianum* (*Cp*, PDB 1CLF), *Thauera aromatica* K172 (*Ta*, PDB 1RGV), *Allochromatium vinosum* (*Av*, PDB 1BLU), and *Pseudomonas aeruginosa* (*Pa*, PDB 2FGO). The multiple alignments were obtained using Clustal Omega program on the webserver (https://www.ebi.ac.uk/Tools/msa/clustalo/).

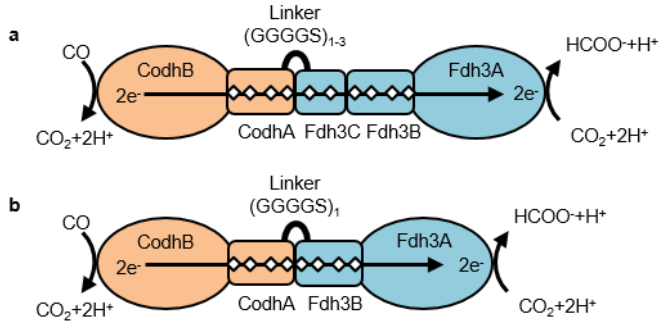

Supplementary Figure 2. Proposed models of synthetic carbon monoxide:formate oxidoreductase (CFOR). a, The fusion constructions of Fdh3C-CodhA with linker $(GGGGS)_{1\text{-}3}$. **b,** The fusion constructions of Fdh3B-CodhA with linker $(GGGGS)_1$.

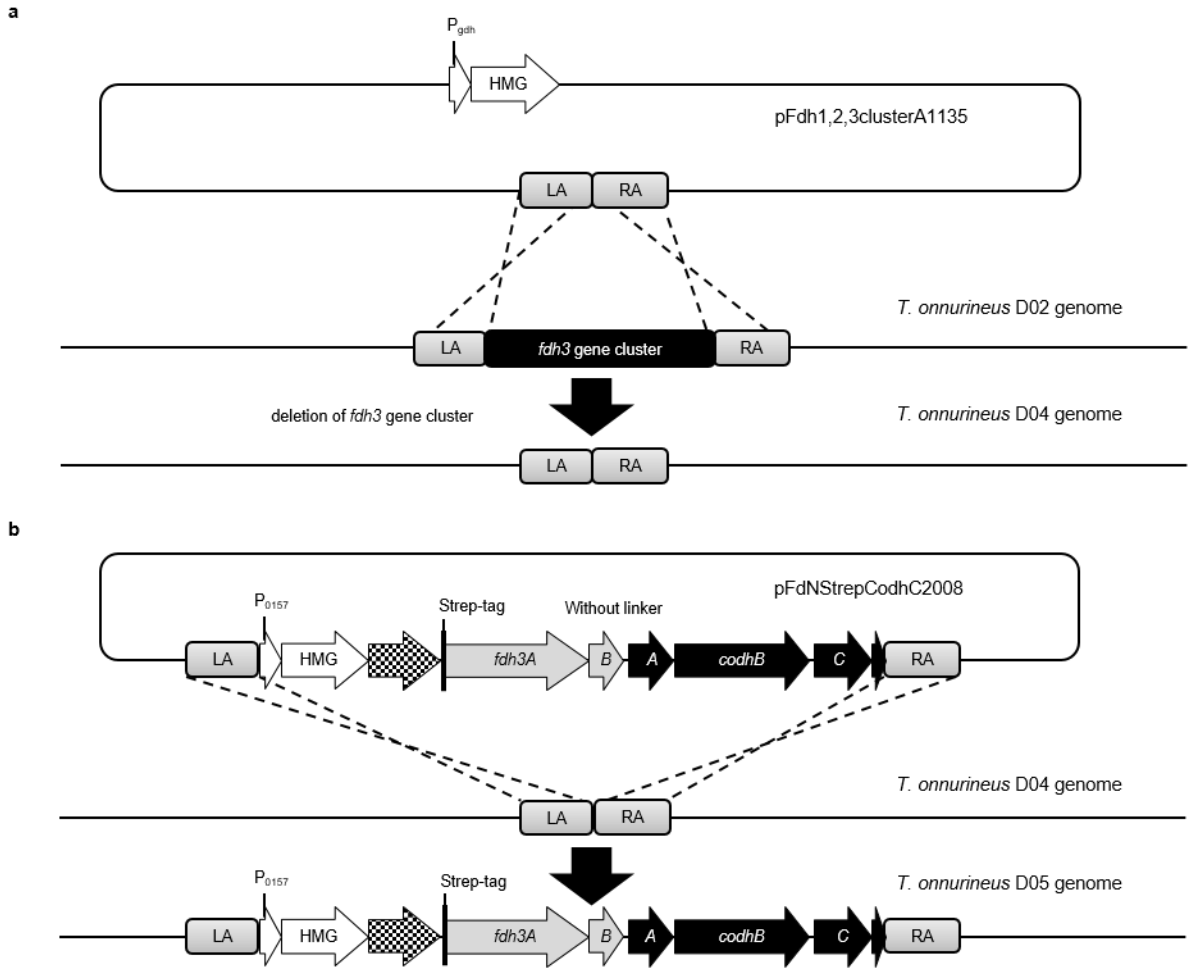

Supplementary Figure 3. Schematic diagram of mutant construction. a, Additional deletion of *fdh3* gene cluster for the construction of *T. onnurineus* D04 strain. Strain D02 was transformed with the pFdh1,2,3clusterA1135 vector containing a fdh3 gene cluster flanked by two ~1 kb DNA fragments, LA (left-arm) and RA (right-arm). Target gene cluster deletion was achieved by double-crossover event. **b,** Construction of *T. onnurineus* D05 mutant by the transformation of pFdNStrepCodhC2008 which has not including flexible linker fusion.

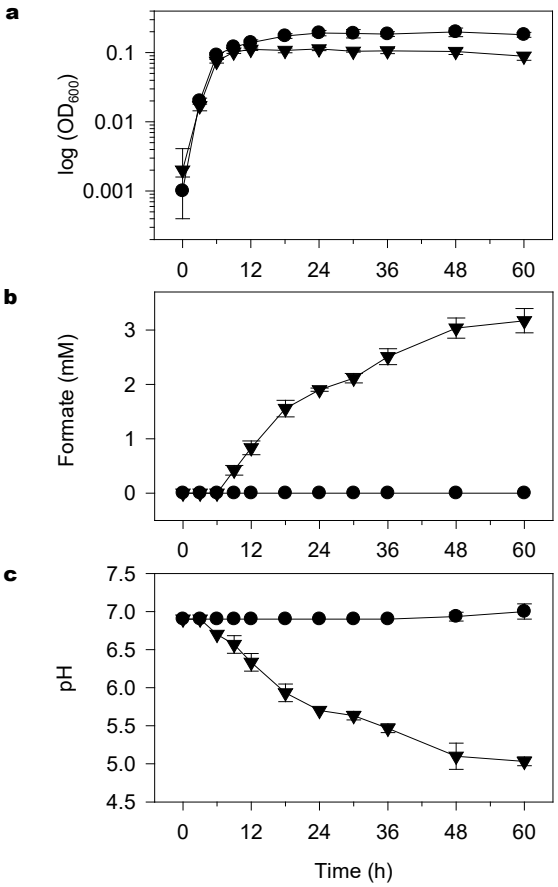

Supplementary Figure 4. Cell growth (a), formate production (b), and pH changes (c) of strain D02 (●) and BCF01 (▼) in 100% CO supplemented serum vials. Error bars represent the standard deviations (n = 3).

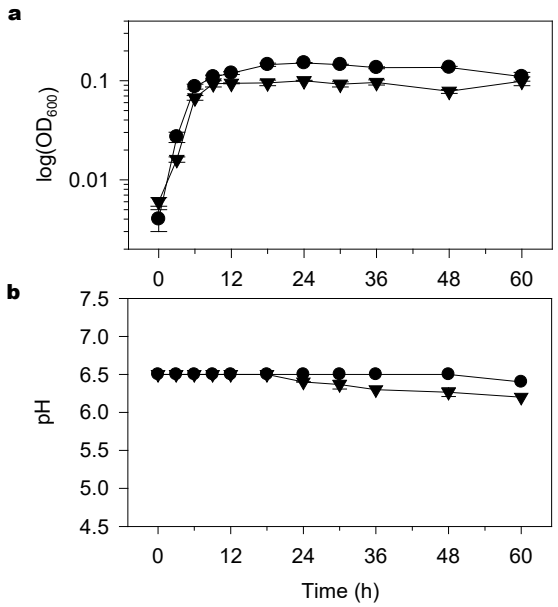

Supplementary Figure 5. Cell growth (a) and pH changes (b) of *T. onnurineus* parental strain D02 (●) and *T. onnurineus* BCF01 (▼), with 0.1 M bis-Tris propane buffer (pH 6.5). Error bars represent the standard deviations (n = 3).

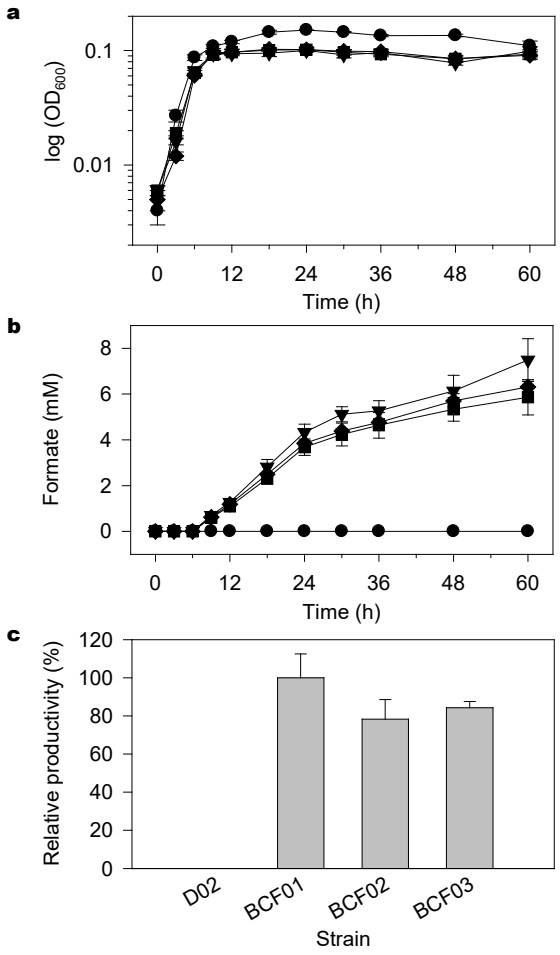

Supplementary Figure 6. CO dependent formate production during serum vial cell growth. a, Cells were incubated at 80℃ with 2 bar of CO gas in serum vial. Cell growth was monitored by measuring OD_{600}. Symbols indicate *T. onnurinues* D02 parental strain (●), BCF01 (▼), BCF02 (■), and BCF03 (◆). **b**, Formate production was measured using HPLC. Symbols are identical to cell growth. **c**, The relative formate productivity at 24 h has compared between BCF01 set to 100% and the other strains. Error bars represent the standard deviations (n = 3).

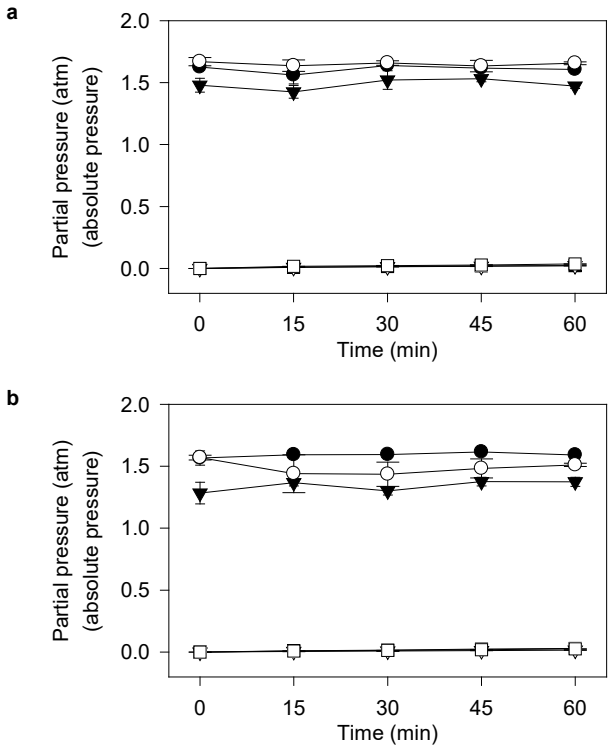

Supplementary Figure 7. Partial pressure changes of *T. onnurineus* BCF 13 (a) and *T. onnurineus* D05 (b) during cell suspension experiments. The headspace was filled with 2 bar (gauge pressure) of CO/CO_2 (50:50 v/v) mix gas (closed symbols) or CO/N_2 (50:50 v/v) mix gas (open symbols). The partial pressure was determined by gas chromatography. Symbols: ● and ○, with P(CO); ▼ and ▽, with $P(CO_2)$; ■ and □,with $P(H_2)$. Error bars represent the standard deviations (n = 3).

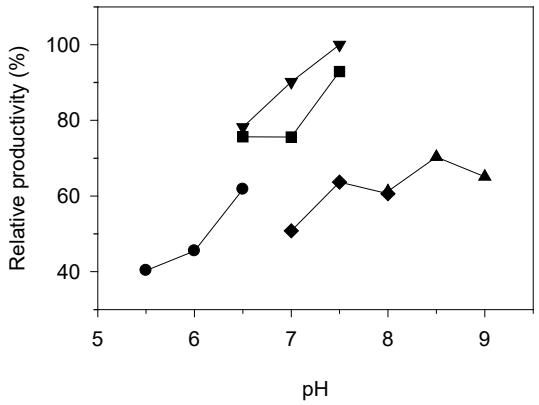

Supplementary Figure 8. Effect of pH on the formate production by the CFOR complex. The activity was assayed at 80°C with CO/CO_2 (50:50 v/v) mix gas. Symbols indicate 50 mM 4-Morpholineethanesulfonic acid (MES) (●), 50 mM sodium phosphate (▼), 50 mM bis-Tris propane propane (■), 4-(2-Hydroxyethyl)piperazine-1-ethanesulfonic acid (HEPES) (◆), and Tris-HCl (▲). Data obtained from one experiment.

Methods

Strains and cell culture conditions

T. onnurineus NA1 wild-type and mutant strains were routinely cultured in modified medium 1 (MM1)[42,43] containing 4g/L of yeast extract (BD Bioscience, San Jose, USA) and 4x Holden's trace element/Fe- EDTA solution at 80℃. All procedures for the cultivation of *T. onnurineus* strains were carried out in an anaerobic chamber (Coy Laboratory Products, Grass Lake, USA). For the cultures in serum bottles, bis-Tris propane (pH 6.5) buffer was additionally supplemented in the medium to a final concentration of 0.1 M, and the headspaces were filled with 100% CO (MMC) was provided to support the growth of wild-type and mutant strains. The serum bottles were sealed with bromobutyl rubber stoppers and aluminum crimp caps. All procedures were carried out under strictly anaerobic conditions.

For the pH-stat batch culture, *T. onnurineus* strain BCF13 was serially cultured in a 150-ml serum bottle and 7 L bioreactors (Fermentec, Cheongwon, South Korea); the working volumes of which were 80 ml and 5 L of MM1 medium, respectively, at 80°C. The bioreactors were sparged with pure argon gas (99.999%) through a microsparger. The agitation speed was 500 rpm, and the pH was controlled at 6.2 using 2 M KOH in 3.5% NaCl. The inlet gas of 100% CO was supplied by using a mass flow controller (MKPrecision, Seoul, South Korea) at feeding rates of 100 - 610 ml/min.

E. coli EPI300^{TM}-T1^{R} (Epicentre Biotechnologies, Madison, USA) strain was used for fosmid based molecular cloning purposes. Fosmid containing *E. coli* clones were cultured in LB medium containing 12.5 ug/ml chloramphenicol. General molecular biology manipulations and microbiological experiments were carried out by standard methods[44].

Cloning and construction of the CFOR expression vector

The cloning strains, plasmids and fosmids used in this study are listed in Supplementary Table 1. The *fdh3* gene cluster deletion mutant (strain D04) was constructed by the previously used gene disruption system in *T. onnurineus* NA1[34] (Supplementary Fig. 3a). To construct fosmid vector backbone, previously constructed complementary insertion site (Left_arm (TON1128-TON_1127) region-P_{0157} promotor-HMG cassette-Right_arm (TON_1126) region)[34] was amplified by PCR using the primers

listed in Supplementary Table 2. The amplicon and fosmid vector pCC1FOS (Epicentre Biotechnologies, Madison, USA) were assembled into a single vector, pNA1comFosC1096 (Supplementary Table 1), using a SLIC method[45]. PCR products of the *T. onnurineus* NA1 Fdh3 encoding gene region (*focA-fdh3ABC* or *focA-fdh3AB*), Codh encoding gene region (*codhABCD*), and fosmid vector backbone (pNA1comFosC1096 with *Avr*II enzyme digestion) were assembled into a single vector using Gibson Assembly Master Mix (New England Biolabs, Ipswich, USA). The fusion targeting Fe-S protein-encoding genes, *fdh3B* or *fdh3C*, and *codhA* from *T. onnurineus* NA1 were fused using a homologous recombination event with 26 bp complementary PCR primers to generate $(GGGGS)_{1-2}$ flexible linker sequence during the gene assembly reaction by the Gibson Assembly method. The 3'-end of *fdh3B* or *fdh3C* gene lacking its stop codon was fused to the 5'-end of *codhA* gene lacking its start codon mediated by $(GGGGS)_{1-2}$ linker (Fig. 1). The sequences of the fusion genes were verified by DNA sequencing. Transformations of *T. onnurineus* strains with the constructed fosmid and the confirmation of transformants were performed as previously described[27]. The primers used to create the fusion genes are listed in Supplementary Table 2.

Analytical methods

Cell growth was monitored by measuring optical density at 600 nm (OD_{600}) with a spectrophotometer (Eppendorf, Hamburg, Germany). The unit value of OD_{600} corresponded to 0.361 g/L (dry cell weight) as previously determined[35]. The amounts of CO, CO_2, and H_2 gas were measured using a gas chromatograph (GC) as described previously[35]. Formate was measured by YL9100 high-performance liquid chromatography (HPLC; YL Instrument Co., Anyang, South Korea) with a Shodex RSpak KC-811 column (Showa Denko, Kanagawa, Japan). Ultrapure water containing 0.1% (v/v) phosphoric acid was used as the mobile phase at a flow rate of 1.0 ml/min. All samples were prepared with 1 ml of culture broth and centrifuged to remove cell debris at 4°C, 13,480 × g for 5 min. The supernatants were purified with a syringe filter and analyzed by HPLC.

Cell suspension experiment

To prepare cell suspensions, *T. onnurineus* strain BCF13 was anaerobically cultured in a 7-L fermentor with a working volume of 3 L as described above. At the end of the culture, the cells were harvested by centrifugation at 5,523 × g for 30 min at 20°C and then washed two times with an anaerobic modified PBS (600 mM NaCl, 2.7 mM KCl, 10 mM Na_2HPO_4, 2 mM KH_2PO_4, and 2 mM DTT). Finally, cells were resuspended in the same buffer at cell densities of OD_{600} = 0.5. Four milliliters of cell suspensions were transferred to a 20-ml serum vial under a headspace of CO/CO_2 (50:50 v/v) mix gas at about 2 bar (gauge pressure), or CO/N_2 (50:50 v/v) mix gas at about 2 bar (gauge pressure), respectively. The cell suspensions were incubated at 80°C, and then the formate concentration and headspace gas composition were determined by HPLC and GC, respectively.

Purification of enzymes

Purification of CFOR enzyme complex was carried out as described previously[46]. Typically 2 to 4 g (wet weight) of fed-batch cultured *T. onnurineus* strain BCF13 cell pellets were harvested and washed with the modified PBS and then resuspended in buffer W (100 mM Tris–HCl, 150 mM NaCl, pH 8.0). Cells were then disrupted by sonication on ice, and cell debris was removed by centrifugation (15,000 x g for 40 min at 4°C). Affinity column purification was carried out following the manufacturer's protocols with a Strep-Tactin system (IBA-Lifsciences, Göttingen, Germany). The molecular weight and additional purification of CFOR complex were determined by analyzing the purified protein on a calibrated Superdex 200 10/300 GL column equilibrated buffer W using fast protein liquid chromatography (Äkta FPLC System, Amersham Biosciences). The column was calibrated by using these standards: thiroglobulin (669 kDa), apoferritin (443 kDa), beta-amylase (200 kDa), albumin (66 kDa) and carbonic anhydrase (29 kDa). Strep-tag purified protein was loaded and eluted at a flow rate of 0.5 ml/min, then the fractions were selectively collected at about 488 kDa of a single peak. The above procedures were carried out under anaerobic conditions. The purified proteins by size exclusion chromatography were used for enzyme assay, and examined via sodium dodecyl sulfate polyacrylamide gel electrophoresis (SDS-PAGE) according to the standard methods. The major bands were identified by LC-MS/MS analysis service (Yonsei Proteome Research Center, Seoul, Korea).

Enzyme assays

CODH activity was assayed at 80°C by a colorimetric assay with methyl viologen (MV) as an electron acceptor (ε_{578} = 9.7 mM/cm at 578 nm)[47], and CO as an electron donor. The assay was conducted with 4.4 ng of purified CFOR complex in 2 ml volume of sodium phosphate buffer (50 mM sodium phosphate, and 2 mM DTT, pH 7.5) containing 5 mM MV in a 4 ml serum-stoppered glass cuvette. 100% CO gas was purged in the headspace at about 2 bar (gauge pressure), and then the reaction was initiated by incubation of the reaction mixture at 80°C. Formate dehydrogenase activity was assayed using 360 ng of purified CFOR complex under the same conditions except that CO was replaced by 10 mM sodium formate. The formate production assay was carried out in 2 ml volume of 50 mM sodium phosphate buffer (pH 7.5) containing 2 mM DTT and 50 ug of purified CFOR in a 20 ml serum-stoppered vial. CO gas was purged in the headspace at about 2 bar (gauge pressure) of CO/CO_2 (50:50 v/v) mix gas, or at about 0.5 bar of 100% CO gas. The reaction was initiated by incubation at 80°C. Formate in reaction mixture was determined by HPLC.

Thermodynamic calculation

The biological standard Gibbs energy value ($\Delta G'^{o}$) was calculated by the Nernst equation using values of the standard Gibbs energy (ΔG^{o}) reported by Amend and Shock[48].